THE JOURNAL OF PHYSICAL CHEMISTRY LETTERS
A JOURNAL OF THE AMERICAN CHEMICAL SOCIETY

pubs.acs.org/JPCL

Letter

Configuration Sensitivity of Electrocatalytic Oxygen Reduction Reaction on Nitrogen-Doped Graphene

Yifan Zhang, Hongquan Fu, Changchun He, Hai Zhang, Yuhang Li, Guangxing Yang, Yonghai Cao, Hongjuan Wang, Feng Peng, Xiaobao Yang,* and Hao Yu*

Cite This: J. Phys. Chem. Lett. 2022, 13, 6187−6193

Read Online

ACCESS | Metrics & More | Article Recommendations | Supporting Information

ABSTRACT: As one of the most promising nonprecious metal catalysts for the oxygen reduction reaction (ORR), the structure of the active site on nitrogen-doped carbon materials is still under debate. Here, we report that the sensitivity of the ORR on the local configuration of multiple nitrogen dopants may be overlooked. Combining global structure searching with density functional theory calculations, we established the structure−activity relationship for 19 and 298 possible configurations of graphitic nitrogen-doped graphene with N content of 2 and 3%, respectively. It was revealed that the stability cannot be a screener to determine the major contributor to the activity. 77.5% of current density is contributed by the active configuration with 4.59% population on the graphene containing 3% nitrogen. It unambiguously demonstrates the configuration sensitivity of N-doped graphene for ORR and opens a new window to identifying the optimal structure of N-doped carbons for various applications.

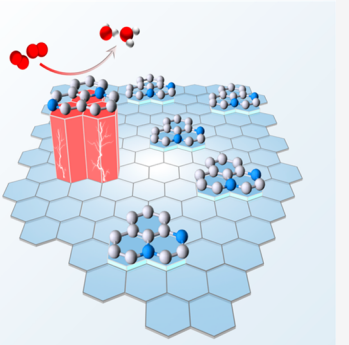

Catalysis is a structure-sensitive phenomenon heavily depending on the local coordination of applied catalyst, which has been validated for heterogeneous catalysis over metals[1,2] and metal oxides,[3,4] single-atom catalysts,[5,6] and enzymic catalysts.[7,8] For instance, the reactivity for a certain reaction over a well-defined metal crystal has been demonstrated to be very different at terrace, steps, kinks, corners, edges, or adatoms for various reactions, which has triggered tremendous efforts to explore the size and shape effects of nanoparticle catalysts.[9−11]

Metal-free carbons with heteroatom dopants have been discovered as an effective catalyst for electrocatalytic oxygen reduction reaction (ORR),[12−14] CO_2 reduction,[15−17] and diverse chemical synthesis[18,19] during the recent decades. Experimental and theoretical studies suggest that the incorporation of heteroatoms redistributes electrons between dopants and surrounding carbon atoms and changes the spin density, thereby endowing carbon with catalytic reactivity.[20−22] Since the nonmetallic dopants are usually in the form of isolated atoms rather than in the forms of crystals or clusters, it is natural that the active sites on doped carbons are highly sensitive to the local coordination, namely, being structure-sensitive. Taking the most investigated nitrogen-doped carboncatalysts as an example, it has been widely accepted that different nitrogen moieties, that is, graphitic/quaternary, pyridinic, and pyrrolic nitrogen, have very different reactivities in ORR. Numerous efforts have been devoted to discriminate those nitrogen species as candidates of active sites. Nevertheless, it is still heavily controversial to identify graphitic[23−26] or pyridinic[27−29] nitrogen as the active site.

The divergent opinions on the active sites require new insights to the structure−reactivity relationship of N-doped carbons for ORR. We stress that (i) a variety of nitrogen species usually coexists on a practical carbon catalyst and (ii) the nitrogen content may be quite high on a practical catalyst to violate the thermodynamic ideality and configurational ideality of Langmuirian adsorption.[30] The former implies that the mutual impact between multiple nitrogen sites should not be ignored. Usachov et al.[31] have shown that the electron doping efficiency of graphitic N can be significantly suppressed by the coexisting pyridinic N. This effect was experimentally verified by directly measuring the electron transfer between carbon surfaces and tetracyanoquinodimethane (TCNQ) as an electron acceptor, which revealed the electronic synergism of graphitic and pyridinic N on ORR activity of N-doped carbon.[32] The latter factor suggests that the clustering effect of N dopants may create a collection of dopants with a new electronic property, defined as a configuration. Obvious segregation of graphitic N sublattice has been observed on N-doped graphene by chemical vapor deposition (CVD)[33] and ion implantation[34] methods. Tison et al.[35] observed the emergence of various nitrogen pairs (1−2, 1−3, 1−4, and 1−8 in a naphthalene structure) on a heavily doped (∼1.3%) but

Received: May 31, 2022
Accepted: June 27, 2022
Published: June 29, 2022

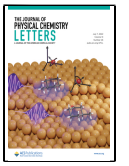

https://doi.org/10.1021/acs.jpclett.2c01645
J. Phys. Chem. Lett. 2022, 13, 6187−6193

graphitic N-dominated graphene and revealed the impact on local electronic property. Some of the complex configurations have been theoretically predicted with a different reactivity.[24,32,36,37]

Those complex configurations of dopants open a new space for the structure−reactivity relationship of N-doped carbons. Unlike the well-defined metal crystals, on which the different but limited sites may be discriminated via geometric approach,[38] the number of possible configurations of dopants may be too large to be affordable for the experimental search when the nitrogen content is high enough for practical applications. To guide the synthesis of high-performance carbon catalysts with a well-defined molecular configuration, a global theoretical study is highly desirable to enumerate all the possible configurations and determine the structure−activity relationship.

Here, we present a density functional theory (DFT) study on the ORR over nitrogen-doped graphene to reveal the configuration-specific reactivity. By applying a searching algorithm with the package of Structures of Alloy Generation And Recognition (SAGAR),[39,40] we generated all nonduplicate configurations. A large graphene supercell of 98 atoms was used for calculations allowing us to investigate the configuration with low nitrogen concentrations in the range from 0% to 3%, which covers the most frequent nitrogen content in the carbon materials synthesized by conventional CVD or thermolysis methods.[41,42] By doing so, the configuration-reactivity relationship of N dopants in graphene was established, which may inspire the rational experimental synthesis of carbon catalysts and, more importantly, provide a deeper insight into the active sites of metal-free carbon catalyst.

Introducing two nitrogen atoms to replace two carbon atoms generates 19 possible configurations (see Table S1 for all the geometries). Figure 1 summarizes the configuration-dependent

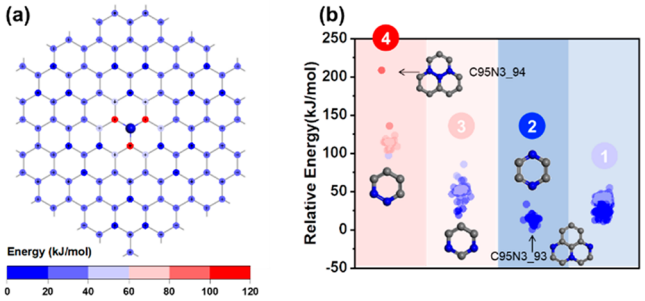

Figure 1. (a) The total energy of C96N2. A graphitic nitrogen atom is fixed in the center. Introducing the second nitrogen atom at a different position results in different total energy, which is represented by the color of the second nitrogen atom. The lowest energy is set to zero. (b) The distribution of total energies of C95N3. The 298 structures are classified into four groups according to their total energy. The characteristic building blocks of C95N3 containing N dopants are illustrated as well. The lateral scattering of the plots within a group is random just for better distinguishing the legends.

total energy of C96N2. The energy reaches the minimum as another nitrogen is doped at the para-position of the same six-membered ring. Meanwhile, the total energy reaches the highest at 102.2 kJ/mol when the second nitrogen atom is placed at the ortho-position,[43] indicating the large repulsion between nitrogen atoms. Most of the other configurations possess the total energy in the range of 9−30 kJ/mol. Figure S1 shows the variation of total energy with the distance between the two nitrogen atoms. Although placing the second nitrogen atom at any positions out of the most adjacent six-membered ring has little effect on the energy, the most stable configuration at the para-position excels others in structural stability by ∼20 kJ/mol. Assuming that the ensembles are in an equilibrium state, the para-configuration (C96N2_8) will be dominant with 47% population.

When three nitrogen atoms are introduced, the number of unduplicated configurations will be boosted to 298. Four groups of C95N3 can be categorized, namely, containing at least one pair of nitrogen at para-, meta-, and ortho-positions (denoted as groups 2, 3, and 4, respectively), and the others without nitrogen atoms in one six-membered ring (denoted as group 1). The existence of para-nitrogen is beneficial for the structural stability. Among them, C95N3_93 (highlighted in Figure 1b) has the lowest total energy, with two pairs of para-nitrogen in two adjacent six-membered rings. The averaged total energy elevates from group 2 to groups 3 and 4, due to the repulsion between two nitrogen atoms in one six-membered ring. Figure S1b summarizes that the energy decreases gradually and changes slowly with the increase of the distance between nitrogen atoms.

The above results clearly uncovered the clustering effect of nitrogen dopants in graphene. The energetic preference to forming para-position nitrogen violates the homogeneous/random assumption of nitrogen distribution in some literature reports,[44,45] suggesting that the dopant atoms tend to form some specific stable configurations, for example, para-nitrogen. Those configurations may be dominant by ∼20 kJ/mol, resulting in their preponderant population at thermodynamical equilibrium.

Nevertheless, the most energetically favorable configuration is not necessarily active for ORR. Hence, we attempted to estimate the ORR overpotential of each configuration aforementioned, starting from computing the adsorption free energies of oxygeneous intermediates (O, OOH, OH). To this end, the active site on each configuration was first determined empirically. O and OH can be adsorbed stably on pristine graphene to form a C−O bond. However, the adsorption of OOH on pure graphene is physical (Figure S2a). Previous studies[27,46−48] have shown that the adsorption of the intermediates near the ortho-carbon of nitrogen is preferential, offering the smaller overpotential; thus, the ortho-carbon of nitrogen dopant is regarded as the active site of ORR. On C97N1 graphene, the intermediates can be chemically adsorbed on the ortho-carbon of nitrogen to form a C−O bond with lower energies. There are multiple ortho-positions in the presence of more than one nitrogen in a supercell. By testing typical C96N2 structures, it was found that the three ortho-carbons of nitrogen have very close ORR overpotentials, which are apparently lower than other carbons (Figure S3). Hence, the ortho-carbon on the side of the other nitrogen atom in C96N2 was chosen as the active site empirically. We treated the ortho-carbons of two nitrogen as two active sites. Twenty-three unduplicated ortho-carbons can be determined for the 19 C96N2 configurations. Analogously, 894 ortho-carbons were computed by considering three active sites for each configuration in the case of C95N3. Table S2 summarizes all the configurations of OH adsorbed on active sites investigated in this work. Figure S4 summarizes the adsorption free energies of oxygeneous intermediates on those active sites.

https://doi.org/10.1021/acs.jpclett.2c01645
J. Phys. Chem. Lett. 2022, 13, 6187−6193

The scaling relationships between ΔG_{OH^*} and ΔG_{OOH^*}, ΔG_{O^*} show good linearity.[49,50]

The overpotential of ORR was calculated from the adsorption free energy of intermediate adsorbent on active sites. Figure 2a,b shows the dependences of overpotential on

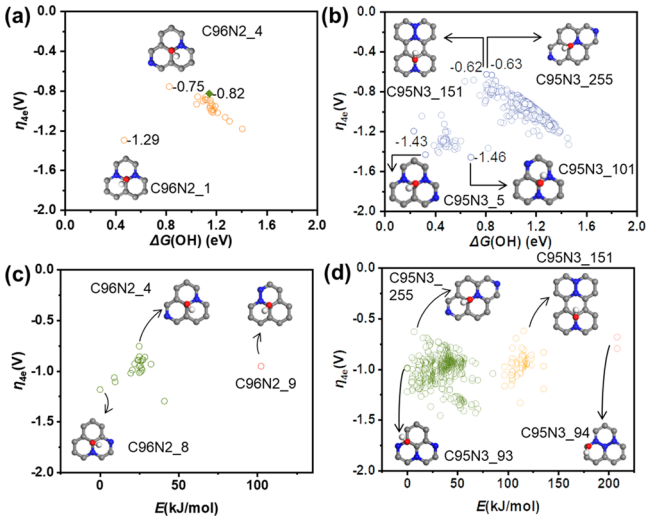

Figure 2. Dependences of overpotential of ORR on the adsorption free energy of OH group on (a) C97N1 (green diamond), C96N2 (orange circle), and (b) C95N3 (blue circle). The dependences of overpotential of ORR on the total energy of (c) C96N2 and (d) C95N3. The green, orange, and red circles represent the graphene without a N−N bond and with one or two N−N bond(s), respectively.

adsorption energy. The volcanic relationships suggest that the approach proposed here can be used to determine the optimal configuration of N-doped graphene for ORR. Both on C96N2 and C95N3 graphene, the lowest overpotential is reached at ΔG_{OH^*} of ∼0.8 eV, being consistent with previous literature.[50−52] On the left and right arms of the volcanic dependences, the ORR is rate-determined by the conversion of OH* to H_2O and O_2 to OOH*, respectively.[50,53] It is interesting to see that the minimal ORR overpotential of C97N1, C96N2, and C95N3 is −0.82, −0.75, and −0.62 V, indicating that it is theoretically feasible to enhance the ORR activity by increasing nitrogen content, which will be discussed in more details later.

The knowledge of the active configurations is helpful for the rational synthesis of carbon catalysts. Among C96N2 graphenes, the most active site is the ortho-carbon adjacent to one nitrogen atom and opposite to the other nitrogen (C96N2_4), as highlighted in Figure 2a. On the contrary, the most inactive structure is C96N2_1 with two meta-nitrogen, which hinders the adsorption of intermediates. By adding one nitrogen to the C96N2 supercell to form C95N3 graphene, the volcanic dependence in Figure 2b suggests that the most active is the one (C95N3_151) adding the extra nitrogen at the ortho-position of one nitrogen in the optimal C96N2 graphene (C96N2_4) or the one (C95N3_255) adding the extra nitrogen at the para-position of nitrogen of C96N2_4. Similarly, the most inactive ones are those adding a nitrogen to C96N2_1, namely, C95N3_5 and C95N3_101. By comparing the results of C96N2 and C95N3 graphene, it can be concluded that adding the third nitrogen atom will not greatly influence the activity if these configurations are already formed. This result re-emphasizes the clustering effect of nitrogen dopants on the ORR activity by forming a specific configuration.

Figure 2c,d reveals the relationship between activity and the structural stability of doping configuration. Overall, the quite scattering plots indicate that the connection between the stability and activity is weak. As shown in Figure 2c, the most stable (lowest total energy) C96N2_8 graphene has a very low activity (high overpotential). The total energy of the most active C96N2_4 graphene is 24.9 kJ/mol higher than that of C96N2_8 graphene, leading to its very low population (see Table S1). Moreover, the C96N2_9 graphene containing a pair of adjacent nitrogen is energetically unfavored, despite its quite low overpotential. The stability-overpotential relationship of C95N3 graphene is displayed in Figure 2d. Depending on the number of N−N bonds in graphene, three collections can be distinguished. Obviously, the N−N bonding significantly elevates the total energy and results in very low population, therefore making them unlikely to be the main contributors of activity, although low overpotentials can be reached over them. Among the relatively stable configurations without N−N bonding, the most stable C95N3_93 graphene performs quite moderately in ORR, while the overpotential can be reduced by 0.354 V over C95N3_255 graphene at the cost of the increase of total energy by 6.9 kJ/mol.

The divergence between stability and reactivity of N-doped graphene makes the prediction of configuration-specific ORR activity misleading to the design of N-doped carbon catalysts. Thermodynamically stable configurations have widely been adopted to discuss the ORR activity and mechanism,[29,46−48,51,52] which may have overlooked the contribution from high-activity configurations. Our results imply that the ORR activity deserves to be reassessed by considering the configuration sensitivity. To mimic practical carbon materials, we assumed that all possible configurations coexist and that the populations distribute in a Boltzmann way. With the ergodic hypothesis in an equilibrium state, the current density can be computed as the ensemble average of the configuration-dependent current densities, namely

$$\overline{j/j_0} = \sum_{n=1,m=1}^{N,M} p_n (j/j_0)_{n,m} \quad (1)$$

where p_n is the population of configuration n, $(j/j_0)_{n,m}$ is the relative current density of active site m on configuration n, N is the number of configurations, and M is the number of active sites. N is 19 or 298, and M is 2 or 3 for C98N2 and C95N3, respectively. By doing so, the polarization curve of the N-doped graphene can be simulated. As shown in Figure 3a, among the 19 C96N2 configurations, the most active (C96N2_4) and most stable (C96N2_8) ones display a huge difference in terms of current density normalized by j_0. The average current density is between the two. It is interesting to analyze the component of the current density. As shown in the inset of Figure 3a, although the most stable C96N2_8 (total energy = 0) occupies 47% population, it contributes 0.5% of the averaged current density. Nevertheless, C96N2_4 (the most active one) and C96N2_16 contribute 32.7% and 30.7% of the average current density with populations of 1.45% and 9.81%, respectively. In the case of C95N3, the ensemble-averaged current density is much higher than that of the most stable C95N3_93, because of the considerable contribution from the minor but active

https://doi.org/10.1021/acs.jpclett.2c01645
J. Phys. Chem. Lett. 2022, 13, 6187−6193

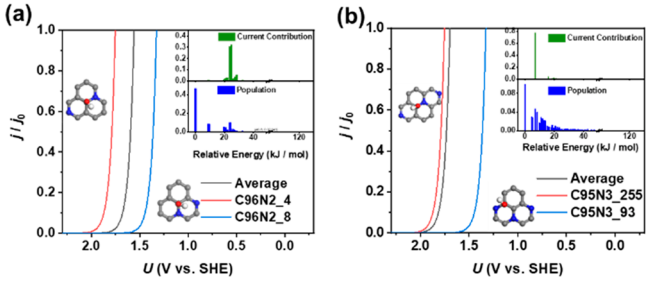

Figure 3. Calculated ORR polarization curves of (a) C96N2 and (b) C95N3. (insets) Population and contribution to current density of all possible configurations.

configurations. In fact, although C95N3_93 graphene has the highest population of 9.92%, its contribution to the current density is negligible (0.33%) because of the inactivity. To our surprise, 77.5% of the current density is from C95N3_255 with 4.59% population (see the inset of Figure 3b), because of its highest activity. These results unambiguously demonstrate the configurational sensitivity of N-doped graphene. On a carbon material without special synthesis strategy (namely, all the configurations are in thermodynamical equilibrium), the majority of the ORR current may be from a rare but active configuration. It challenges not only the theoretical prediction based on a DFT calculation of the thermodynamically stable configuration but also the experimental identification of active site on carbons via microscopy and spectroscopy,[29,54] because the frequently observed configuration may be not the major contributor of activity, as revealed in Figure 3b.

The insight into the structure−activity relationship indicates that the activity of N-doped carbon is ensemble-specific. It allows us to evaluate the effect of N content on the ORR current density on a specific ensemble. For the ensemble in thermodynamic equilibrium, the polarization curves of C97N1, C96N2, and C95N3 in Figure S5 display that, as the N content increased from ∼1% to ∼2%, the ORR current density decreased; while the N content is increased to ∼3%, a slightly higher activity can be obtained. The abnormal variation of activity with N content violates the common belief that increasing N content is beneficial for the reactivity. Although the ORR overpotential on the optimal configuration decreases with the N content as revealed in Figure 2, the comprehensive investigation through the ensemble of all possible configurations shows the complex result. It emphasizes that the emergence of new active configurations as increasing the number of dopants, due to the clustering effect, significantly changes the catalytic performance of N-doped carbon catalysts. This result may explain why the ORR activity cannot be reproduced well on N-doped carbon materials from a different laboratory by various syntheses.

The nitrogen doping temperature affects the population of configurations and, thereby, the ORR reactivity. As summarized in Figure S5b, the current density of C96N2 graphene gradually increases with the temperature from 250 to 1500 K. eq 2 indicates that, when the temperature rises, the population of the configuration with high energy will increase. Therefore, the contribution from the most active structure (C96N2_4) increases in the case of C96N2, which in turn improves the overall activity, while the current density on C95N3 graphene increases first and then decreases, maximizing at 550 K. It can be rationalized by the high populations of high-energy configurations but with low activities that suppress the overall current density. This result further indicates that the clustering effect enables the formation of a specific configuration that contributes dominantly to the reactivity when doping nitrogen at controlled temperatures, thereby improving the overall reactivity.

In summary, a new paradigm was proposed to evaluate the ORR activity of N-doped graphene by globally searching all the possible configurations of N-dopants and establishing the structure−activity relationship. By doing so, the populations of 19 C96N2 and 298 C95N3 configurations were determined using the total energy as a measure, which reveals the clustering effect of N dopants, namely, the preference forming energetically favorable configurations containing para-nitrogen. Assuming the ortho-carbon of nitrogen as active sites, the adsorption free energies of OH, O, and OOH intermediates were calculated to determine the ORR overpotential in the frame of an associative mechanism. The structure−activity relationship enables one to search for the optimal configuration of N atoms to guide the synthesis of high-performance N-doped carbon materials. The configuration sensitivity of N doping was uncovered by analyzing the fractional contribution to the Faraday current. For instance, the rare configuration C95N3_255 (4.59% population) may contribute 77.5% current density of C95N3 graphene. Although the preliminary work constrained the N dopant as the graphitic type with N content less than 3%, which is a good approximation to the N-doped carbon materials with a high graphitization degree annealed at high temperatures,[41,42] the findings disclose a key factor to elucidate the catalytic performance of N-doped carbon catalysts and pave a new avenue to a rational design and synthesis of carbon materials for ORR and other related applications.

METHODOLOGY

Models. We used Materials Studio's modeling tool (Materials Visualizer) to construct a periodic graphene supercell composed of 98 carbon atoms, with the lattice parameters of a = 17.22 Å and b = 17.22 Å. To minimize the interaction between different layers, a vacuum region of 16 Å was set up between layers. Graphitic nitrogen dopants were introduced into the graphene structure by replacing one to three carbon atoms with nitrogen atoms, corresponding to the atomic content of nitrogen from 0% to 3.06%. Multiple configurations are possible when more than one nitrogen atom is introduced into the supercell, which can be determined using the SAGAR package previously developed.[39,40] In this work, 19 and 298 nonduplicated configurations are modeled in the cases of introducing 2 and 3 nitrogen atoms, respectively, allowing for an unbiased evaluation. All the models are visualized in Table S1, denoted as CnNm_i, where n, m are the numbers of carbon and nitrogen atoms in the supercell, respectively, and i is the serial number of the models.

Theoretical Calculations. Each configuration was geometry-optimized, and the total energy was calculated in the DMol^3 module of Materials Studio software, where the term total energy refers to the energy of a specific arrangement of atoms. The zero of energy is taken to be the infinite separation of all electrons and nuclei; thus, the total energy is generally negative, corresponding to a bound state. The total energies of structures with the same atoms reveal their structural stability.

The total energy can be a measure of probability density at which a specific configuration appears when the N-doping is thermodynamically driven. In this way, the probability density

https://doi.org/10.1021/acs.jpclett.2c01645
J. Phys. Chem. Lett. 2022, 13, 6187−6193

of a particular configuration i could be given by its Boltzmann population p_i:

$$p_i = \frac{g_i e^{-E_i/kT}}{\sum_i g_i e^{-E_i/kT}} \quad (2)$$

where g_i is the degenerate energy level of i generated by SAGAR, E_i is the total energy of i from DFT calculation, T is the nitrogen doping temperature (1073 K), and k is Boltzmann constant. See details in the Supporting Information.

Estimation of ORR Overpotential and Current Density. The ORR is assumed to follow the associative mechanism,[24,50] in which O_2 is not decomposed but directly converted to the OOH* intermediate. The overpotential of ORR can be determined by comparing the reaction free energy of each elementary step. For each step, the reaction free energy is defined as the difference between the initial state and the final state[55]

$$\Delta G = \Delta E - T\Delta S + \Delta \mathrm{ZPE} + eU \quad (3)$$

where ΔE is the energy change of reactant and product molecules. According to the calculated hydrogen electrode model,[56] the chemical potential of proton−electron pairs can be expressed by the chemical potential of hydrogen molecules on the assumption that the electric potential is zero when it is neutral. U is the potential of the electrode. T is the temperature. e is the transferred charge. The change of zero vibration energy and the change of entropy are calculated by the frequency from the DMol^3 module.

The ORR limit potential is the minimum of limit potentials.

$$\Delta U_L = \min(\Delta U_{L1}, \Delta U_{L2}, \Delta U_{L3}, \Delta U_{L4}) \quad (4)$$

The ORR overpotential is

$$\eta = 1.23 - \Delta U_L \quad (5)$$

The Butler−Volmer equation gives the current density as

$$j = Fk^0[C_O(0, t)e^{-\alpha f\eta} - C_R(0, t)e^{(1-\alpha)f\eta}] \quad (6)$$

where F is Faraday's constant, k^0 is the standard rate constant of reaction, C_O (0,t) and C_R (0,t) are surface concentrations, f is calculated as F/RT, where T is 298 K, α is a transfer coefficient which is 0.5, and η is the overpotential. Introducing the exchange current density j_0, the current density can be written as

$$j = j_0\left[\frac{C_O(0, t)}{C_O^*}e^{-\alpha f\eta} - \frac{C_R(0, t)}{C_R^*}e^{(1-\alpha)f\eta}\right] = j[e^{-\alpha f\eta} - e^{(1-\alpha)f\eta}] \quad (7)$$

where the first item is the cathode current

$$j/j_0 = e^{-\alpha f\eta} \quad (8)$$

See details in the Supporting Information.

■ ASSOCIATED CONTENT

Supporting Information

The Supporting Information is available free of charge at https://pubs.acs.org/doi/10.1021/acs.jpclett.2c01645.

Detailed computational methods, calculation results, and other additional information (PDF)

■ AUTHOR INFORMATION

Corresponding Authors

Xiaobao Yang − *School of Physics, South China University of Technology, Guangzhou 510641, China;* orcid.org/0000-0001-8851-1988; Email: scxbyang@scut.edu.cn

Hao Yu − *School of Chemistry and Chemical Engineering, Guangdong Provincial Key Lab of Green Chemical Product Technology, South China University of Technology, Guangzhou 510641, China;* orcid.org/0000-0003-2862-8054; Email: yuhao@scut.edu.cn

Authors

Yifan Zhang − *School of Chemistry and Chemical Engineering, Guangdong Provincial Key Lab of Green Chemical Product Technology, South China University of Technology, Guangzhou 510641, China*

Hongquan Fu − *Chemical Synthesis and Pollution Control Key Laboratory of Sichuan Province, China West Normal University, Nan-chong 637000, China;* orcid.org/0000-0001-5474-7052

Changchun He − *School of Physics, South China University of Technology, Guangzhou 510641, China*

Hai Zhang − *School of Chemistry and Chemical Engineering, Guangdong Provincial Key Lab of Green Chemical Product Technology, South China University of Technology, Guangzhou 510641, China*

Yuhang Li − *School of Chemistry, Sun Yat-sen University, Guangzhou 510275, China*

Guangxing Yang − *School of Chemistry and Chemical Engineering, Guangdong Provincial Key Lab of Green Chemical Product Technology, South China University of Technology, Guangzhou 510641, China*

Yonghai Cao − *School of Chemistry and Chemical Engineering, Guangdong Provincial Key Lab of Green Chemical Product Technology, South China University of Technology, Guangzhou 510641, China;* orcid.org/0000-0003-0035-6253

Hongjuan Wang − *School of Chemistry and Chemical Engineering, Guangdong Provincial Key Lab of Green Chemical Product Technology, South China University of Technology, Guangzhou 510641, China*

Feng Peng − *School of Chemistry and Chemical Engineering, Guangzhou University, Guangzhou 510006, China;* orcid.org/0000-0002-5154-6666

Complete contact information is available at: https://pubs.acs.org/10.1021/acs.jpclett.2c01645

Notes

The authors declare no competing financial interest.

■ ACKNOWLEDGMENTS

This work was supported by the National Natural Science Foundation of China (Nos. 21906058, 21978107, and 21676100), Guangdong Basic and Applied Basic Research Foundation (Nos. 2021A1515010112 and 2017A030312005), and Science and Technology Program of Guangzhou City (No. 202002030287). The DFT calculations were carried out at the National Supercomputer Center in Guangzhou.

■ REFERENCES

(1) Whittell, G. R.; Hager, M. D.; Schubert, U. S.; Manners, I. Functional Soft Materials from Metallopolymers and Metallosupramolecular Polymers. *Nat. Mater.* **2011**, *10* (3), 176−188.

(2) Simmons, T. R.; Berggren, G.; Bacchi, M.; Fontecave, M.; Artero, V. Mimicking Hydrogenases: From Biomimetics to Artificial Enzymes. *Coord. Chem. Rev.* **2014**, *270*−*271*, 127−150.
(3) Blasco, T.; Nieto, J. M. L. Oxidative Dyhydrogenation of Short Chain Alkanes on Supported Vanadium Oxide Catalysts. *Appl. Catal., A* **1997**, *157* (1), 117−142.
(4) Pelletier, J. D. A.; Basset, J.-M. Catalysis by Design: Well-Defined Single-Site Heterogeneous Catalysts. *Acc. Chem. Res.* **2016**, *49* (4), 664−677.
(5) Zhang, H.; Liu, G.; Shi, L.; Ye, J. Single-Atom Catalysts: Emerging Multifunctional Materials in Heterogeneous Catalysis. *Adv. Energy Mater.* **2018**, *8* (1), 1701343.
(6) Sun, Y.; Gao, S.; Lei, F.; Xie, Y. Atomically-Thin Two-Dimensional Sheets for Understanding Active Sites in Catalysis. *Chem. Soc. Rev.* **2015**, *44* (3), 623−636.
(7) Fallarino, F.; Grohmann, U.; Puccetti, P. Indoleamine 2,3-Dioxygenase: From Catalyst to Signaling Function. *Eur. J. Immunol.* **2012**, *42* (8), 1932−1937.
(8) Campbell, A. P.; Tarasow, T. M.; Massefski, W.; Wright, P. E.; Hilvert, D. Binding of a High-Energy Substrate Conformer in Antibody Catalysis. *Proc. Natl. Acad. Sci. U. S. A.* **1993**, *90* (18), 8663.
(9) Narayanan, R.; El-Sayed, M. A. Catalysis with Transition Metal Nanoparticles in Colloidal Solution: Nanoparticle Shape Dependence and Stability. *J. Phys. Chem. B* **2005**, *109* (26), 12663−12676.
(10) Campbell, C. T.; Parker, S. C.; Starr, D. E. The Effect of Size-Dependent Nanoparticle Energetics on Catalyst Sintering. *Science* **2002**, *298* (5594), 811−814.
(11) Guo, S.; Zhang, S.; Sun, S. Tuning Nanoparticle Catalysis for the Oxygen Reduction Reaction. *Angew. Chem., Int. Ed.* **2013**, *52* (33), 8526−8544.
(12) Shao, M.; Chang, Q.; Dodelet, J.-P.; Chenitz, R. Recent Advances in Electrocatalysts for Oxygen Reduction Reaction. *Chem. Rev.* **2016**, *116* (6), 3594−3657.
(13) Zhang, J.; Zhao, Z.; Xia, Z.; Dai, L. A Metal-Free Bifunctional Electrocatalyst for Oxygen Reduction and Oxygen Evolution Reactions. *Nat. Nanotechnol.* **2015**, *10* (5), 444−452.
(14) Li, Y.; Zhao, Y.; Cheng, H.; Hu, Y.; Shi, G.; Dai, L.; Qu, L. Nitrogen-Doped Graphene Quantum Dots with Oxygen-Rich Functional Groups. *J. Am. Chem. Soc.* **2012**, *134* (1), 15−18.
(15) Kumar, B.; Asadi, M.; Pisasale, D.; Sinha-Ray, S.; Rosen, B. A.; Haasch, R.; Abiade, J.; Yarin, A. L.; Salehi-Khojin, A. Renewable and Metal-Free Carbon Nanofibre Catalysts for Carbon Dioxide Reduction. *Nat. Commun.* **2013**, *4* (1), 2819.
(16) Wu, J.; Yadav, R. M.; Liu, M.; Sharma, P. P.; Tiwary, C. S.; Ma, L.; Zou, X.; Zhou, X.-D.; Yakobson, B. I.; Lou, J.; et al. Achieving Highly Efficient, Selective, and Stable CO_2 Reduction on Nitrogen-Doped Carbon Nanotubes. *ACS Nano* **2015**, *9* (5), 5364−5371.
(17) Duan, X.; Xu, J.; Wei, Z.; Ma, J.; Guo, S.; Wang, S.; Liu, H.; Dou, S. Metal-Free Carbon Materials for CO_2 Electrochemical Reduction. *Adv. Mater.* **2017**, *29* (41), 1701784.
(18) Murugesan, K.; Donabauer, K.; König, B. Visible-Light-Promoted Metal-Free Synthesis of (Hetero)Aromatic Nitriles from C(sp3)-H Bonds. *Angew. Chem., Int. Ed.* **2021**, *60* (5), 2439−2445.
(19) Zhao, S.; Lu, X.; Wang, L.; Gale, J.; Amal, R. Carbon-Based Metal-Free Catalysts for Electrocatalytic Reduction of Nitrogen for Synthesis of Ammonia at Ambient Conditions. *Adv. Mater.* **2019**, *31* (13), 1805367.
(20) Qu, L.; Liu, Y.; Baek, J.-B.; Dai, L. Nitrogen-Doped Graphene as Efficient Metal-Free Electrocatalyst for Oxygen Reduction in Fuel Cells. *ACS Nano* **2010**, *4* (3), 1321−1326.
(21) Jiang, H.; Wang, Y.; Hao, J.; Liu, Y.; Li, W.; Li, J. N and P Co-Functionalized Three-Dimensional Porous Carbon Networks as Efficient Metal-Free Electrocatalysts for Oxygen Reduction Reaction. *Carbon* **2017**, *122*, 64−73.
(22) Borghei, M.; Laocharoen, N.; Kibena-Poldsepp, E.; Johansson, L.-S.; Campbell, J.; Kauppinen, E.; Tammeveski, K.; Rojas, O. J. Porous N,P-Doped Carbon from Coconut Shells with High Electrocatalytic Activity for Oxygen Reduction: Alternative to Pt-C for Alkaline Fuel Cells. *Appl. Catal., B* **2017**, *204*, 394−402.
(23) Yang, H. B.; Miao, J. W.; Hung, S. F.; Chen, J. Z.; Tao, H. B.; Wang, X. Z.; Zhang, L. P.; Chen, R.; Gao, J. J.; Chen, H. M.; et al. Identification of Catalytic Sites for Oxygen Reduction and Oxygen Evolution in N-Doped Graphene Materials: Development of Highly Efficient Metal-Free Bifunctional Electrocatalyst. *Sci. Adv.* **2016**, *2* (4). DOI: 10.1126/sciadv.1501122
(24) Ma, R.; Lin, G.; Zhou, Y.; Liu, Q.; Zhang, T.; Shan, G.; Yang, M.; Wang, J. A Review of Oxygen Reduction Mechanisms for Metal-Free Carbon-Based Electrocatalysts. *npj Comput. Mater.* **2019**, *5* (1), 78.
(25) Watanabe, H.; Asano, S.; Fujita, S.; Yoshida, H.; Arai, M. Nitrogen-Doped, Metal-Free Activated Carbon Catalysts for Aerobic Oxidation of Alcohols. *ACS Catal.* **2015**, *5* (5), 2886−2894.
(26) Wang, N.; Lu, B.; Li, L.; Niu, W.; Tang, Z.; Kang, X.; Chen, S. Graphitic Nitrogen Is Responsible for Oxygen Electroreduction on Nitrogen-Doped Carbons in Alkaline Electrolytes: Insights from Activity Attenuation Studies and Theoretical Calculations. *ACS Catal.* **2018**, *8* (8), 6827−6836.
(27) Guo, D.; Shibuya, R.; Akiba, C.; Saji, S.; Kondo, T.; Nakamura, J. Active Sites of Nitrogen-Doped Carbon Materials for Oxygen Reduction Reaction Clarified Using Model Catalysts. *Science* **2016**, *351* (6271), 361.
(28) Takeyasu, K.; Furukawa, M.; Shimoyama, Y.; Singh, S. K.; Nakamura, J. Role of Pyridinic Nitrogen in the Mechanism of the Oxygen Reduction Reaction on Carbon Electrocatalysts. *Angew. Chem., Int. Ed. Engl.* **2021**, *60* (10), 5121−5124.
(29) Xing, T.; Zheng, Y.; Li, L.; Cowie, B.; Gunzelmann, D.; Qiao, S.; Huang, S.; Chen, Y. Observation of Active Sites for Oxygen Reduction Reaction on Nitrogen-Doped Multilayer Graphene. *ACS Nano* **2014**, *8* (7), 6856−6862.
(30) Razdan, N. K.; Bhan, A. Catalytic Site Ensembles: A Context to Reexamine the Langmuir-Hinshelwood Kinetic Description. *J. Catal.* **2021**, *404*, 726−744.
(31) Usachov, D.; Fedorov, A.; Vilkov, O.; Senkovskiy, B.; Adamchuk, V. K.; Yashina, L. V.; Volykhov, A. A.; Farjam, M.; Verbitskiy, N. I.; Grüneis, A.; et al. The Chemistry of Imperfections in N-Graphene. *Nano Lett.* **2014**, *14* (9), 4982−4988.
(32) Ning, X.; Li, Y.; Ming, J.; Wang, Q.; Wang, H.; Cao, Y.; Peng, F.; Yang, Y.; Yu, H. Electronic Synergism of Pyridinic- and Graphitic-Nitrogen on N-Doped Carbons for the Oxygen Reduction Reaction. *Chem. Sci.* **2019**, *10* (6), 1589−1596.
(33) Zabet-Khosousi, A.; Zhao, L.; Pálová, L.; Hybertsen, M. S.; Reichman, D. R.; Pasupathy, A. N.; Flynn, G. W. Segregation of Sublattice Domains in Nitrogen-Doped Graphene. *J. Am. Chem. Soc.* **2014**, *136* (4), 1391−1397.
(34) Telychko, M.; Mutombo, P.; Ondráček, M.; Hapala, P.; Bocquet, F. C.; Kolorenč, J.; Vondráček, M.; Jelínek, P.; Švec, M. Achieving High-Quality Single-Atom Nitrogen Doping of Graphene/SiC(0001) by Ion Implantation and Subsequent Thermal Stabilization. *ACS Nano* **2014**, *8* (7), 7318−7324.
(35) Tison, Y.; Lagoute, J.; Repain, V.; Chacon, C.; Girard, Y.; Rousset, S.; Joucken, F.; Sharma, D.; Henrard, L.; Amara, H.; et al. Electronic Interaction between Nitrogen Atoms in Doped Graphene. *ACS Nano* **2015**, *9* (1), 670−678.
(36) Li, J.; Yin, S.; Dong, F.; Cen, W.; Chu, Y. Tailoring Active Sites Via Synergy between Graphitic and Pyridinic N for Enhanced Catalytic Efficiency of a Carbocatalyst. *ACS Appl. Mater. Interfaces* **2017**, *9* (23), 19861−19869.
(37) Fu, H.; Huang, K.; Yang, G.; Cao, Y.; Wang, H.; Peng, F.; Wang, Q.; Yu, H. Synergistic Effect of Nitrogen Dopants on Carbon Nanotubes on the Catalytic Selective Epoxidation of Styrene. *ACS Catal.* **2020**, *10* (1), 129−137.
(38) Le Valant, A.; Bouchet, S.; Van Assche, A.; Especel, C.; Epron, F. Description of Supported Metal Structure Sensitivity by a Geometric Approach. *J. Catal.* **2021**, *397*, 64−74.
(39) Cheng, Y.; Liao, J.; Zhao, Y.; Ni, J.; Yang, X. Theoretical Investigations on Stable Structures of $C_{60-n}N_n$ (n = 2−12): Symmetry, Model Interaction, and Global Optimization. *Carbon* **2019**, *154*, 140−149.

https://doi.org/10.1021/acs.jpclett.2c01645
J. Phys. Chem. Lett. 2022, 13, 6187−6193

(40) He, C.-C.; Qiu, S.-B.; Yu, J.-S.; Liao, J.-H.; Zhao, Y.-J.; Yang, X.-B. Atom Classification Model for Total Energy Evaluation of Two-Dimensional Multicomponent Materials. *J. Phys. Chem. A* **2020**, *124* (22), 4506−4511.
(41) Batzill, M. The Surface Science of Graphene: Metal Interfaces, CVD Synthesis, Nanoribbons, Chemical Modifications, and Defects. *Surf. Sci. Rep.* **2012**, *67* (3), 83−115.
(42) Wei, D.; Liu, Y.; Wang, Y.; Zhang, H.; Huang, L.; Yu, G. Synthesis of N-Doped Graphene by Chemical Vapor Deposition and Its Electrical Properties. *Nano Lett.* **2009**, *9* (5), 1752−1758.
(43) Hou, M.; Zhang, X.; Yuan, S.; Cen, W. Double Graphitic-N Doping for Enhanced Catalytic Oxidation Activity of Carbocatalysts. *Phys. Chem. Chem. Phys.* **2019**, *21* (10), 5481−5488.
(44) Zhang, S.; Tsuzuki, S.; Ueno, K.; Dokko, K.; Watanabe, M. Upper Limit of Nitrogen Content in Carbon Materials. *Angew. Chem., Int. Ed. Engl.* **2015**, *54* (4), 1302−1306.
(45) Zhou, Y.; Yang, Y.; Hou, G.; Yi, D.; Zhou, B.; Chen, S.; Lam, T. D.; Yuan, F.; Golberg, D.; Wang, X. Stress-Relieving Defects Enable Ultra-Stable Silicon Anode for Li-Ion Storage. *Nano Energy* **2020**, *70*, 104568.
(46) Jiang, H.; Gu, J.; Zheng, X.; Liu, M.; Qiu, X.; Wang, L.; Li, W.; Chen, Z.; Ji, X.; Li, J. Defect-Rich and Ultrathin N Doped Carbon Nanosheets as Advanced Trifunctional Metal-Free Electrocatalysts for the ORR, OER and HER. *Energy Environ. Sci.* **2019**, *12* (1), 322−333.
(47) Duan, Z.; Henkelman, G. Identification of Active Sites of Pure and Nitrogen-Doped Carbon Materials for Oxygen Reduction Reaction Using Constant-Potential Calculations. *J. Phys. Chem. C* **2020**, *124* (22), 12016−12023.
(48) Wang, T.; Chen, Z.-X.; Chen, Y.-G.; Yang, L.-J.; Yang, X.-D.; Ye, J.-Y.; Xia, H.-P.; Zhou, Z.-Y.; Sun, S.-G. Identifying the Active Site of N-Doped Graphene for Oxygen Reduction by Selective Chemical Modification. *ACS Energy Lett.* **2018**, *3* (4), 986−991.
(49) Wang, Q.; Ji, Y.; Lei, Y.; Wang, Y.; Wang, Y.; Li, Y.; Wang, S. Pyridinic-N-Dominated Doped Defective Graphene as a Superior Oxygen Electrocatalyst for Ultrahigh-Energy-Density Zn-Air Batteries. *ACS Energy Lett.* **2018**, *3* (5), 1183−1191.
(50) Kulkarni, A.; Siahrostami, S.; Patel, A.; Norskov, J. K. Understanding Catalytic Activity Trends in the Oxygen Reduction Reaction. *Chem. Rev.* **2018**, *118* (5), 2302−2312.
(51) Liu, Z.; Zhao, Z.; Wang, Y.; Dou, S.; Yan, D.; Liu, D.; Xia, Z.; Wang, S. In Situ Exfoliated, Edge-Rich, Oxygen-Functionalized Graphene from Carbon Fibers for Oxygen Electrocatalysis. *Adv. Mater.* **2017**, *29* (18). DOI: 10.1002/adma.201606207
(52) Tao, L.; Qiao, M.; Jin, R.; Li, Y.; Xiao, Z.; Wang, Y.; Zhang, N.; Xie, C.; He, Q.; Jiang, D.; et al. Bridging the Surface Charge and Catalytic Activity of a Defective Carbon Electrocatalyst. *Angew. Chem., Int. Ed. Engl.* **2019**, *58* (4), 1019−1024.
(53) Nørskov, J. K.; Rossmeisl, J.; Logadottir, A.; Lindqvist, L.; Kitchin, J. R.; Bligaard, T.; Jónsson, H. Origin of the Overpotential for Oxygen Reduction at a Fuel-Cell Cathode. *J. Phys. Chem. B* **2004**, *108* (46), 17886−17892.
(54) Jin, H.; Huang, H.; He, Y.; Feng, X.; Wang, S.; Dai, L.; Wang, J. Graphene Quantum Dots Supported by Graphene Nanoribbons with Ultrahigh Electrocatalytic Performance for Oxygen Reduction. *J. Am. Chem. Soc.* **2015**, *137* (24), 7588−7591.
(55) Wang, Z.-L.; Xu, D.; Xu, J.-J.; Zhang, X.-B. Oxygen Electrocatalysts in Metal-Air Batteries: From Aqueous to Nonaqueous Electrolytes. *Chem. Soc. Rev.* **2014**, *43* (22), 7746−7786.
(56) Kitchin, J. R.; Norskov, J. K.; Barteau, M. A.; Chen, J. G. Modification of the Surface Electronic and Chemical Properties of Pt(111) by Subsurface 3d Transition Metals. *J. Chem. Phys.* **2004**, *120* (21), 10240.

https://doi.org/10.1021/acs.jpclett.2c01645
J. Phys. Chem. Lett. 2022, 13, 6187−6193